Report

Cell Reports

ELAC1 Repairs tRNAs Cleaved during Ribosome-Associated Quality Control

Graphical Abstract

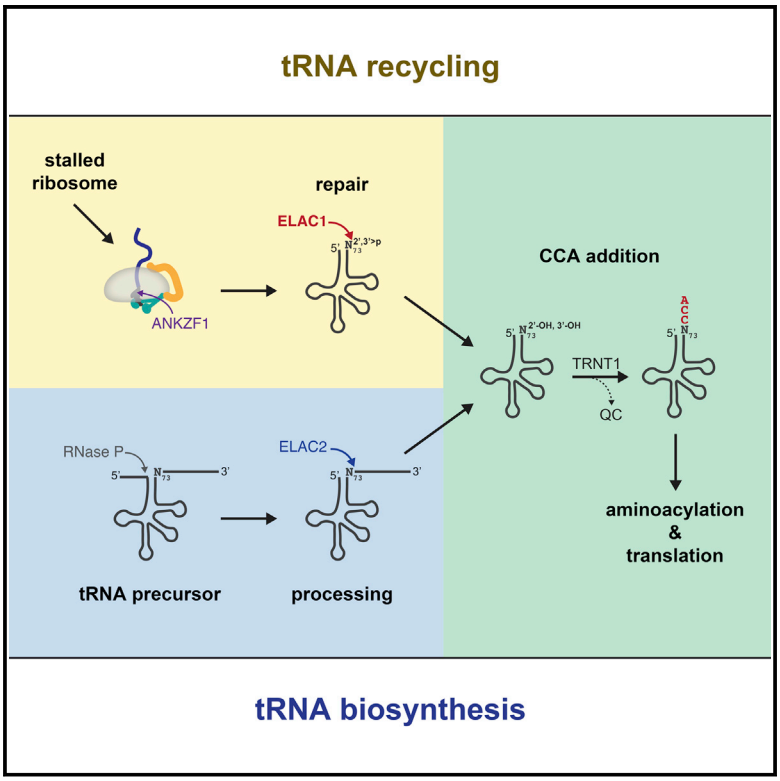

Authors

Matthew C.J. Yip, Simonas Savickas, Steven P. Gygi, Sichen Shao

Correspondence

sichen_shao@hms.harvard.edu

In Brief

Yip et al. identify ELAC1 as a tRNA repair enzyme that is necessary and sufficient to remove 2′,3′-cyclic phosphates from tRNAs cleaved by ANKZF1 on stalled ribosomes to permit 3′CCA re-addition and tRNA recycling.

Highlights

- ANKZF1 cleaves off the 3′CCA of peptidyl-tRNAs on stalled ribosomes
- A 2′,3′-cyclic phosphate must be removed from ANKZF1-cleaved tRNAs for recycling
- ELAC1 is necessary and sufficient to repair ANKZF1-cleaved tRNAs for CCA addition
- ELAC1 activity is specialized for tRNA repair over tRNA biogenesis

Yip et al., 2020, Cell Reports *30*, 2106–2114
February 18, 2020
https://doi.org/10.1016/j.celrep.2020.01.082

CellPress

OPEN ACCESS
CellPress

Cell Reports
Report

ELAC1 Repairs tRNAs Cleaved during Ribosome-Associated Quality Control

Matthew C.J. Yip,[1] Simonas Savickas,[1,2] Steven P. Gygi,[1] and Sichen Shao[1,3,*]
[1]Department of Cell Biology, Blavatnik Institute, Harvard Medical School, Boston, MA 02115, USA
[2]Department of Biotechnology and Biomedicine, Technical University of Denmark, Kgs. Lyngby, Denmark
[3]Lead Contact
*Correspondence: sichen_shao@hms.harvard.edu
https://doi.org/10.1016/j.celrep.2020.01.082

SUMMARY

Ribosome-associated quality control (RQC) disassembles aberrantly stalled translation complexes to recycle or degrade the constituent parts. A key step of RQC is the cleavage of P-site tRNA by the endonuclease ANKZF1 (Vms1 in yeast) to release incompletely synthesized polypeptides from ribosomes for degradation. Re-use of the cleaved tRNA for translation requires re-addition of the universal 3′CCA nucleotides removed by ANKZF1. Here, we show that ELAC1 is both necessary and sufficient to remove the 2′,3′-cyclic phosphate on ANKZF1-cleaved tRNAs to permit CCA re-addition by TRNT1. ELAC1 activity is optimized for tRNA recycling, whereas ELAC2, the essential RNase Z isoform in eukaryotes, is required to remove 3′ trailers during tRNA biogenesis. Cells lacking ELAC1 specifically accumulate unrepaired tRNA intermediates upon the induction of ribosome stalling. Thus, optimal recycling of ANKZF1-cleaved tRNAs in vertebrates is achieved through the duplication and specialization of a conserved tRNA biosynthesis enzyme.

INTRODUCTION

Protein synthesis is an energetically demanding process that is tightly regulated to ensure fidelity. Ribosomes that slow excessively or stall during translation signify a potential problem that initiates quality control and recycling mechanisms to resolve the stalled ribosomal complexes. Some components of stalled translational complexes, such as the partially synthesized nascent polypeptide and mRNA, are considered by the cell to be faulty and degraded (Lykke-Andersen and Bennett, 2014; Shoemaker and Green, 2012). Other components, such as the ribosomal subunits and tRNAs, are thought to be recycled. The cell would ideally check these components for structural and functional integrity before re-use, but the specific mechanisms that recycle translational factors are not fully understood.

When considering how cells handle aberrant translational complexes, we have the clearest understanding of the ribosome-associated quality control (RQC) pathway leading to nascent protein degradation (Joazeiro, 2019). RQC relies on the dissociation of stalled ribosomes into 60S and 40S ribosomal subunits, which frees the mRNA for degradation and traps the nascent peptidyl-tRNA on the 60S subunit (Brandman et al., 2012; Shao et al., 2013; Shoemaker et al., 2010). NEMF/Rqc2 selectively binds the interface of this 60S-peptidyl-tRNA complex and helps recruit the ubiquitin ligase Listerin/Ltn1 to polyubiquitinate the nascent protein (Bengtson and Joazeiro, 2010; Lyumkis et al., 2014; Shao et al., 2015; Shen et al., 2015). Subsequent extraction and proteasomal degradation of nascent proteins from 60S RQC complexes involves ANKZF1/Vms1, the AAA ATPase p97/Cdc48, and TCF25/Rqc1 (Defenouillère et al., 2013; Verma et al., 2013, 2018; Zurita Rendón et al., 2018). Impaired RQC results in proteotoxicity and neurodegeneration in model systems (Choe et al., 2016; Chu et al., 2009; Izawa et al., 2017), highlighting the importance of removing faulty translational substrates and products in maintaining cellular homeostasis.

Cells may also scrutinize the translation factors on aberrant ribosomal complexes. Supporting this idea are links between ribosome splitting factors and nonfunctional rRNA decay pathways (Cole et al., 2009; Limoncelli et al., 2017; Sugiyama et al., 2019). In the case of tRNAs, recent studies (Kuroha et al., 2018; Yip et al., 2019) demonstrated that RQC complex disassembly does not simply liberate free tRNA as previously thought (Verma et al., 2018; Zurita Rendón et al., 2018). Instead, ANKZF1/Vms1 is an endonuclease (Kuroha et al., 2018) that cleaves off the universally conserved 3′CCA nucleotides (positions 74–76) of peptidyl-tRNA on 60S-RQC complexes (Yip et al., 2019). ANKZF1 cleavage releases nascent proteins for degradation (Verma et al., 2018; Zurita Rendón et al., 2018) and simultaneously generates a tRNA intermediate containing a 2′,3′-cyclic phosphate (2′,3′>p) on the ribose of the discriminator base at position 73 (N_{73}) that is incompatible with translation. Recycling of ANKZF1-cleaved tRNAs occurs efficiently in the mammalian cytosol through a two-step process (Yip et al., 2019): removal of the 2′,3′>p followed by the re-addition of the 3′CCA by the CCA-adding enzyme TRNT1. How ANKZF1-cleaved tRNAs with 2′,3′>p are repaired for CCA addition is not known.

Using activity-guided biochemical fractionations, we identify ELAC1 (tRNase Z^S) as the mammalian factor that is necessary and sufficient to remove the 2′,3′>p of ANKZF1-cleaved tRNAs to permit recycling. ELAC1 is one of two RNase Z (also called ELAC for homologs of bacterial ElaC) isoforms found in

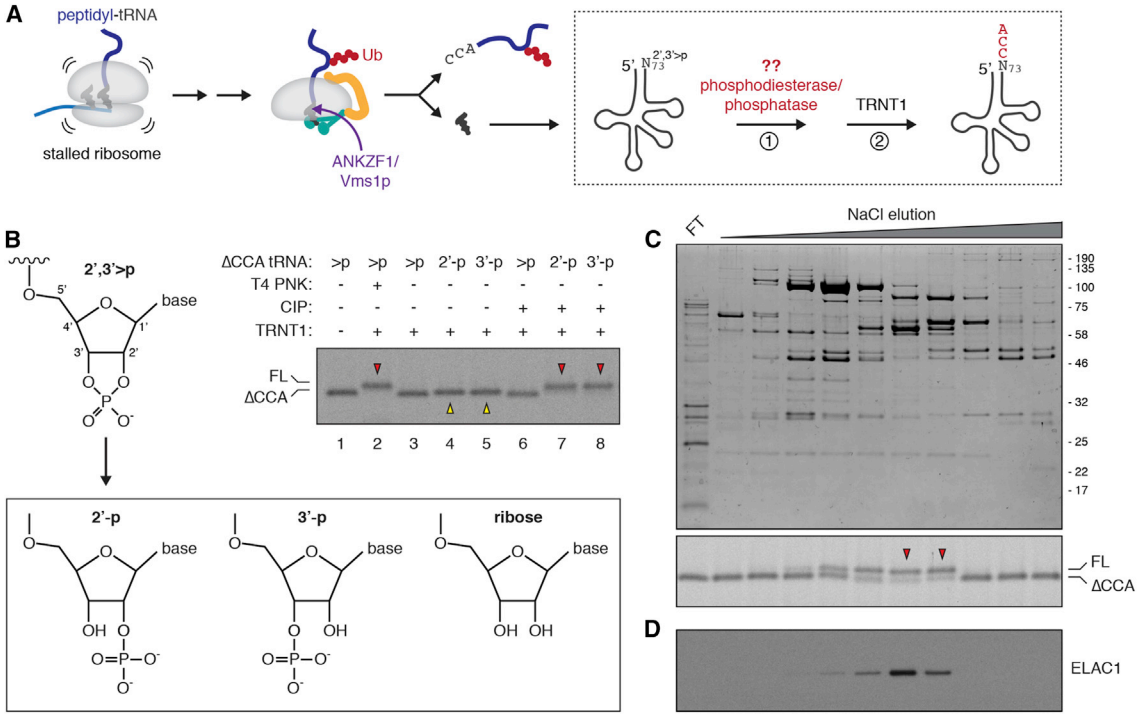

Figure 1. Requirements of Repairing ANKZF1-Cleaved tRNAs for CCA Addition

(A) During ribosome-associated quality control (RQC), stalled ribosomes are dissociated to 60S and 40S ribosomal subunits. The 60S-peptidyl-tRNA complex is recognized by NEMF (teal) and Listerin (orange), which mediates polyubiquitination (Ub) of the nascent protein. ANKZF1 (purple) cleavage of the peptidyl-tRNA generates a ΔCCA tRNA with a 2′,3′-cyclic phosphate (2′,3′>p) on the discriminator base (N_{73}) that must be resolved before TRNT1 is able to add back the 3′CCA nucleotides (red).

(B) A total of 2 ng/μL of *in-vitro*-transcribed radiolabeled leucyl-tRNA lacking the 3′CCA nucleotides appended to the hepatitis delta virus ribozyme (ΔCCA-HDV) was incubated with nothing to maintain a 2′,3′>p (>p), T4 PNK to generate 2′ and 3′ hydroxyl groups, CNP to generate a 2′ phosphate (2′-p), or RtcB to generate a 3′ phosphate (3′-p) on N_{73}. The ΔCCA tRNA products were incubated with 100 nM TRNT1 and nucleotides directly (lanes 2–5) or after treatment with calf intestinal alkaline phosphatase (CIP) (lanes 6–8). The reactions were analyzed by SDS-PAGE and autoradiography to assay for the addition of 3′CCA nucleotides producing full-length (FL; red arrowheads) tRNA. Yellow arrowheads denote slower migration of ΔCCA tRNAs without a 2′,3′>p.

(C) Coomassie stain (top) of flow-through (FT) or salt-eluted fractions of reticulocyte lysate from heparin resin. Individual fractions were incubated with radiolabeled ΔCCA-HDV and TRNT1 to assay for FL tRNA production (bottom). Fractions with peak activity (red arrowheads) were pooled for further analyses.

(D) Immunoblot of ELAC1 distribution through the fractions shown in (C).

See also Figure S1 and Table S1.

eukaryotes (Aravind, 1999). RNase Z enzymes generally function to cleave off 3′ trailer sequences from tRNA precursors, leaving a 3′-hydroxy (3′-OH) group on N_{73} (Vogel et al., 2005). RNase Z cleavage generates substrates for TRNT1 to add on the 3′CCA nucleotides, which are not genetically encoded in many bacterial and all eukaryotic tRNAs (Phizicky and Hopper, 2010). Although ELAC2 (tRNase Z^L) is essential for tRNA biogenesis in all eukaryotes (Brzezniak et al., 2011; Dubrovsky et al., 2004; Siira et al., 2018), ELAC1 is found primarily in vertebrates and plants (Fan et al., 2011; Wang et al., 2012) and its function is poorly characterized. Our results reveal a specialization of RNase Z activity for tRNA repair.

RESULTS

CCA Addition Requires Complete Removal of 2′,3′>p from tRNA substrates

In earlier work, we established that ANKZF1-cleaved tRNAs contain a 2′,3′>p on the discriminator nucleotide at position 73 (N_{73}) that precludes CCA re-addition by TRNT1 (Yip et al., 2019; Figure 1A). To identify the physiologic pathway to CCA addition, we determined which possible processing products of 2′,3′>p are competent for CCA addition by TRNT1. To mimic ANKZF1-cleaved tRNA, we transcribed a CCA-less leucyl-tRNA fused to the hepatitis delta virus ribozyme (ΔCCA-HDV) (Figure S1A). The HDV ribozyme cleaves itself from the preceding transcript to leave a 2′,3′>p on the ΔCCA tRNA (Schürer et al., 2002). The 2′,3′>p can be resolved to three possible products: 2′-phosphate (2′-p) and 3′-OH, 2′-OH and 3′-p, or 2′-OH and 3′-OH (Figure 1B). We generated each of these products by enzymatic treatment of radiolabeled ΔCCA-HDV and monitored CCA addition by TRNT1 by gel electrophoresis.

As we previously demonstrated (Yip et al., 2019), converting the 2′,3′>p to 2′-OH and 3′-OH by using bacteriophage T4 PNK (polynucleotide kinase) permits CCA addition to generate full-length (FL) tRNA (Figure 1B, lane 2). In contrast, conversion to 2′-p and 3′-OH by using CNP (2′,3′-cyclic-nucleotide 3′

phosphodiesterase) did not support CCA addition (lane 4). Conversion to 2′-OH and 3′-p using the *Escherichia coli* RtcB ligase also precluded CCA addition (lane 5). Subsequent treatment with CIP (calf intestinal alkaline phosphatase), which hydrolyzes phosphomonoester (but not cyclic phosphodiester) bonds, reestablished the ability to recycle ΔCCA tRNAs with a 2′-p or 3′-p (lanes 7 and 8), but not a 2′,3′>p (lane 6). Thus, recycling of ANKZF1-cleaved tRNAs by TRNT1 requires full conversion of the 2′,3′>p to 2′-OH and 3′-OH. This may be accomplished by a single enzyme (as with T4 PNK) or through the sequential actions of a phosphodiesterase and phosphatase.

A Specific Factor Removes 2′,3′>p from ΔCCA tRNAs

Although a two-step repair mechanism for ΔCCA tRNAs with 2′,3′>p involving a eukaryotic phosphodiesterase and phosphatase is possible *in vitro* (Figure 1B), these enzymes are unlikely to comprise the physiological tRNA repair pathway. CNP is primarily expressed in the central nervous system (Raasakka and Kursula, 2014), and alkaline phosphatase activity is extracellular (Coleman, 1992). Because cytosol from mammalian cells efficiently recycles ANKZF1-cleaved tRNAs (Yip et al., 2019), we took an activity-guided fractionation approach to identify the endogenous factor(s) that remove the 2′,3′>p on ANKZF1-cleaved tRNAs. To do this, we biochemically fractionated rabbit reticulocyte lysate and followed the 2′,3′>p repair activity by monitoring CCA addition to radiolabeled ΔCCA-HDV by TRNT1 (Figure 1C; Figure S1B).

Repair activity was maintained in single peaks through four fractionation steps (Figure 1C; Figures S1C–S1G). This suggests that one protein or protein complex removes the 2′,3′>p rather than the sequential action of separate phosphodiesterase and phosphatase activities. Label-free mass spectrometry analysis of a fraction enriched for 2′,3′-cyclic phosphatase activity returned a list of 23 proteins (Table S1). Among these hits was ELAC1, which we chose to analyze further based on the function of its homologs in generating substrates for CCA addition during tRNA biogenesis (Vogel et al., 2005).

ELAC1 Is Necessary and Sufficient to Repair ANKZF1-Cleaved tRNAs for CCA Addition

ELAC1 abundance correlated with ΔCCA-HDV repair activity through our biochemical fractionations (Figure 1D; Figures S1C–S1E). Purified recombinant ELAC1 repaired ΔCCA-HDV for CCA addition by TRNT1 as efficiently as T4 PNK (Figure 2A, lanes 4–9). A single point mutation (H64A) that disrupts the active site of ELAC1 abolished repair activity (lane 10). Thus, ELAC1 is sufficient to repair 2′,3′>p on ΔCCA-HDV and co-fractionates with the sole repair activity in reticulocyte lysate, arguing that this is at least one physiological repair pathway for 2′,3′>p in mammals.

We next tested whether ELAC1 and TRNT1 were sufficient to recycle peptidyl-tRNAs cleaved by ANKZF1/Vms1 during RQC (Figure 2B). As described previously (Shao and Hegde, 2014), we produced stalled ribosome-nascent protein complexes (RNCs) by *in vitro* translation of a truncated (i.e., nonstop) mRNA and affinity purified the RNCs by an epitope tag on the nascent polypeptide. These purified RNCs contain endogenous valyl-tRNA in the P-site attached to the nascent polypeptide. Incubation with purified ribosome splitting factors and NEMF generates a 60S-NEMF complex containing an intact peptidyl-tRNA (Shao et al., 2015; Yip et al., 2019), which served as the starting point for our downstream analysis (Figure 2B, diagram).

Relative to a starting sample containing intact FL tRNA (Figure 2B, top panel, lane 1), including Vms1 produced a cleaved ΔCCA tRNA product (lane 2) that migrates faster by gel electrophoresis. The addition of TRNT1 did not convert Vms1-cleaved ΔCCA tRNA back to FL tRNA (lane 3) unless ELAC1 (lane 4) or T4 PNK (lane 6) was also included. Recycled FL tRNA specifically incorporated radiolabeled cytidine (lanes 4 and 6, bottom panel), verifying that repair occurred. Importantly, enzymatically inactive ELAC1(H64A) did not support CCA re-addition by TRNT1 (lane 5), and wild-type ELAC1 had no effect in the absence of TRNT1 (lane 7). Thus, ELAC1 is sufficient to repair native tRNAs cleaved in the context of RQC for CCA re-addition.

To determine if ELAC1 is the major enzyme mediating tRNA repair, we isolated cytosolic lysates from wild-type and ELAC1 knockout cells and assayed their ability to recycle ΔCCA-HDV (Figure 2C; Figure S2). Knocking out ELAC1 impaired tRNA recycling (Figure 2C, lanes 3, 4, and 7), similar to knocking down TRNT1 (lane 2). The defect of removing ELAC1 was specifically rescued by adding back wild-type recombinant ELAC1 (lanes 5 and 8), but not the H64A mutant (lanes 6 and 9). ELAC1 is, therefore, necessary and sufficient to remove 2′,3′>p from ΔCCA tRNAs for recycling.

ELAC1 Activity Is Specialized for tRNA Repair

The observation that removing ELAC1 disrupts tRNA recycling was unexpected considering the potentially redundant activity of ELAC2. Although present in our lysates (Figure S2), ELAC2 apparently cannot compensate for ELAC1 function in tRNA repair (Figure 2C). ELAC1, like bacterial ElaC, resides as homodimers in the cytosol, where the tRNA-binding exosite of one ELAC1 subunit positions substrates in the active site of the other subunit (Takahashi et al., 2008; Figure 3A; Figure S3A). ELAC2 is thought to have evolved from an ELAC1 gene duplication and fusion and functions as a monomer (Tavtigian et al., 2001). The N-terminal domain lacks catalytic activity but retains the tRNA-binding exosite to position substrates for cleavage by the C-terminal domain. Alternative translation initiation sites control the expression of a mitochondrial localization sequence to distribute ELAC2 between the nucleus and mitochondria (Rossmanith, 2011), the two sites of tRNA biosynthesis. The primary function of ELAC2 of cleaving 3′ trailers from pre-tRNA intermediates during tRNA biogenesis is universally conserved across eukaryotes. In comparison, our analysis indicates that ELAC1 functions to remove 2′,3′>p from tRNA intermediates generated by ribosome stalling.

We investigated this apparent difference between the two human ELAC isoforms by comparing the activities of purified recombinant ELAC1 and ELAC2 in 2′,3′>p removal versus cleavage of a 13 nucleotide 3′ trailer for CCA addition. *In vitro* transcribed and radiolabeled ΔCCA-HDV or ΔCCA-trailer (pre) was incubated with either ELAC1 or ELAC2, and successful processing was assayed by the generation of FL tRNA by TRNT1. ELAC1 efficiently removed 2′,3′>p from ΔCCA-HDV (Figure 3B, top left panel) but could not cleave ΔCCA-trailer (bottom left panel). In

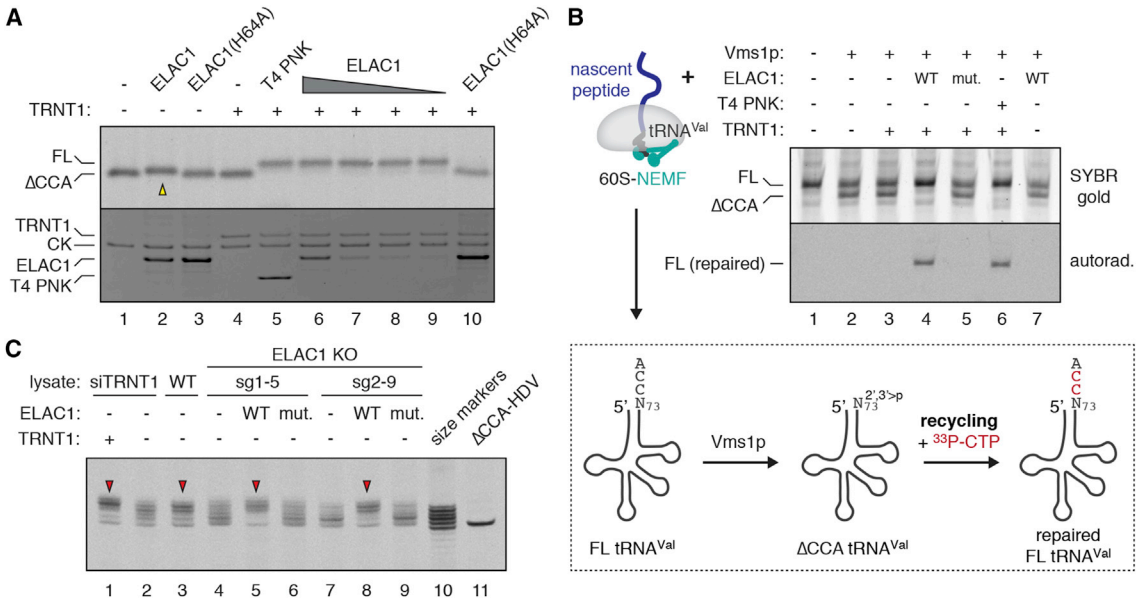

Figure 2. ELAC1 Is Necessary and Sufficient for tRNA Repair

(A) A total of 2-ng/μL-radiolabeled ΔCCA-HDV was incubated as indicated with wild-type (WT) ELAC1 or ELAC1(H64A), 100 nM TRNT1, 0.375 U/μL T4 PNK, and nucleotides. Conversion of ΔCCA to FL tRNA was assayed by SDS-PAGE and autoradiography (top panel). Coomassie staining is shown below. Yellow arrowhead denotes slower migration of ΔCCA tRNA with 2′-OH and 3′-OH groups relative to ΔCCA tRNA with a 2′,3′>p. CK, creatine kinase in the energy regeneration system.

(B) Stalled ribosome-nascent protein complexes (RNCs) were affinity purified from *in vitro* translation reactions of a nonstop mRNA truncated at a valine codon. A total of 5 nM RNCs was incubated with an energy regenerating system, recombinant ribosome splitting factors, 10 nM NEMF, and 0.2 mM [α-^{33}P]-CTP with or without 125 nM Vms1, 100 nM WT or H64A (mutant [mut.]) ELAC1, TRNT1, and/or T4 PNK as indicated. Isolated RNAs were analyzed by 15% Tris-borate-EDTA (TBE)-urea-PAGE and SYBR gold staining (top panel) or autoradiography (bottom panel) to detect cleavage of and CCA addition to endogenous valyl-tRNA. FL and cleaved (ΔCCA) valyl-tRNAs are labeled.

(C) Hypotonic lysates from TRNT1 knockdown (siTRNT1), WT, or ELAC1 knockout (KO) HEK293T cells generated with different guide RNA sequences were incubated with 20-ng/μL-radiolabeled ΔCCA-HDV without or with 100 nM TRNT1 and 20 nM WT or mut. ELAC1. Extracted RNAs were analyzed by 15% TBE-urea-PAGE and autoradiography. Red arrowheads denote conditions that yield WT levels of tRNA recycling. Size markers (lane 10) mark the migration of FL leucyl-tRNA and leucyl-tRNA lacking one to four 3′ terminal nucleotides. Results are representative of experiments with four different ELAC1 KO cell lines.

See also Figure S2.

contrast, ELAC2 efficiently cleaved ΔCCA-trailer but displayed weaker ability to repair ΔCCA-HDV (Figure 3B, right panels), instead preferentially hydrolyzing only one of the phosphoester bonds (Figure S3B, lanes 10 and 11). Trz1, the sole ELAC enzyme in yeast, performed both activities comparably (Figure S3C). Thus, yeast also contain repair activity for tRNAs cleaved during RQC.

An analysis of different 3′ tRNA trailer lengths (Figure S3D) showed that ELAC1 cleavage activity drops off sharply between a trailer length of 2 to 5 nucleotides (Figure 3C). In contrast, ELAC2 and Trz1 could cleave trailers of all lengths examined. This difference in cleavage efficiency is consistent with previous observations of ELAC1 and ELAC2 tRNA 3′ processing activities (Takaku et al., 2003; Yan et al., 2006). Because most precursor tRNAs are transcribed with trailers of 8 to 15 nucleotides (Gogakos et al., 2017), our observations support the idea that ELAC1 is not a major contributor to tRNA biogenesis. Consistent with this model, lysates lacking ELAC1 were not impaired in processing ΔCCA-trailer (Figure S3E).

Unlike T4 PNK, ELAC1 is not a promiscuous 2′,3′-cyclic phosphatase. When presented with tRNA-HDV substrates containing two additional nucleotides between N_{73} and the HDV ribozyme, ELAC1 still precisely cleaved 3′ of N_{73} (Figure S3F, lane 3), whereas T4 PNK only removed the 2′,3′>p on the terminal nucleotide at position 75 (lane 2). This result is consistent with the conserved mechanism for positioning N_{73} of tRNA substrates in the active site of ELAC enzymes (Li de la Sierra-Gallay et al., 2006). As a consequence, T4 PNK converted tRNA-HDV with two cytidine, but not adenine, nucleotides following N_{73} to a TRNT1 substrate for the addition of the terminal adenine of the 3′CCA (lane 6). In contrast, ELAC1 reset both tRNA-HDV substrates for CCA addition (lane 7). ELAC1 is also able to break a phosphomonoester bond at either the 2′ or 3′ position of N_{73} of ΔCCA tRNA (Figure S3G) and does not require a substrate with a 2′,3′>p. The ability to recognize and act on the ribose of N_{73} of tRNA substrates, combined with the capacity to convert a variety of starting products to the exact substrate for CCA addition, specifically tailors ELAC1 function for tRNA repair (Figure 3D).

ELAC1 Is Required to Recycle tRNAs in Mammalian Cells during Ribosome Stalling

The duplication of ELAC enzymes in vertebrates and their specialized functions in tRNA biogenesis versus repair provided a unique opportunity to investigate the consequences of

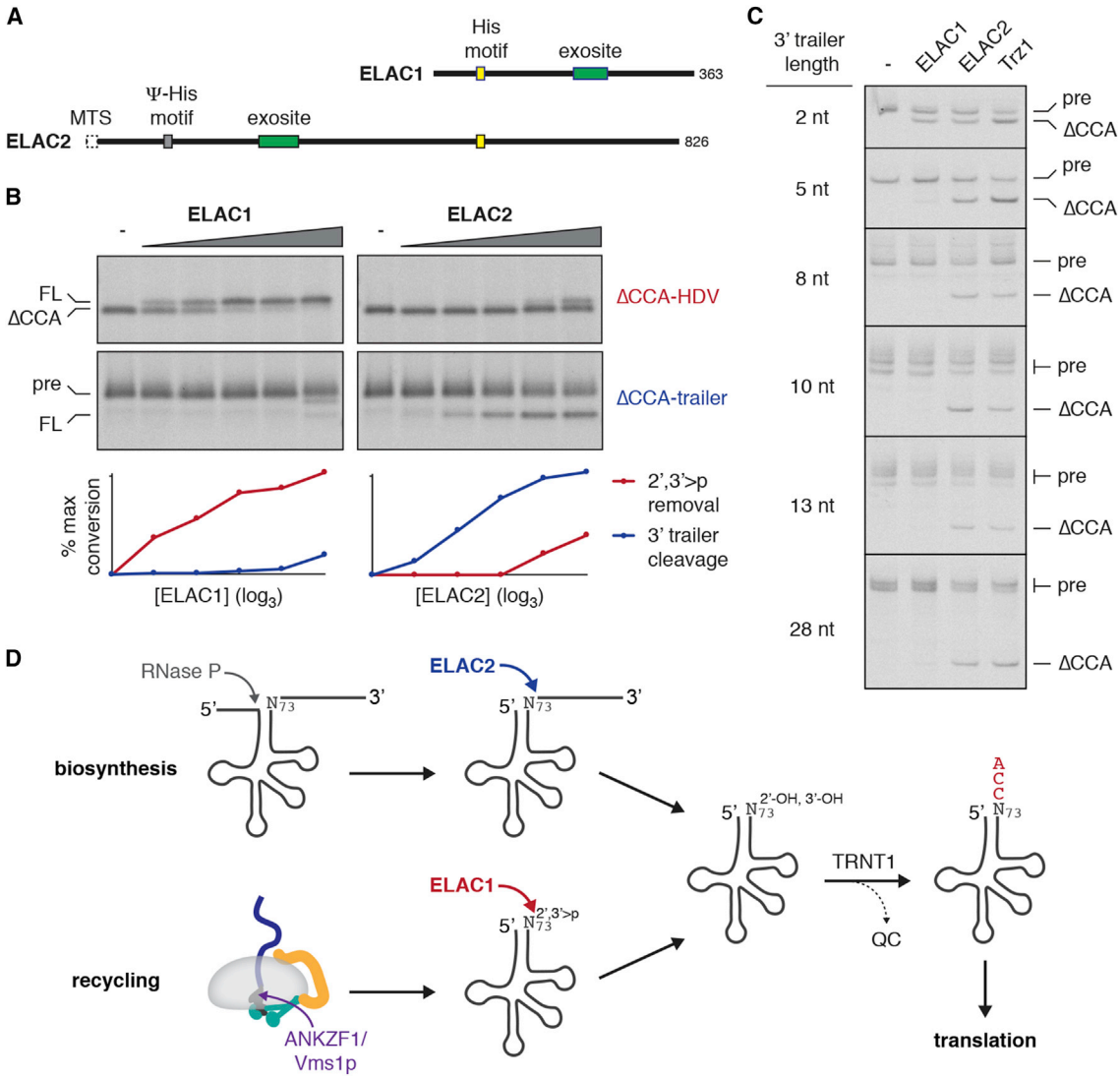

Figure 3. Specialization of Mammalian ELAC Isoforms for tRNA Repair or Biosynthesis

(A) Domain structures of mammalian ELAC isoforms. Locations of catalytic His motif (yellow), catalytically inactive pseudo-His (ψ-His, gray), and tRNA-binding exosite (green) motifs are indicated. MTS, mitochondrial targeting sequence.

(B) Comparison of the 2′,3′>p removal and 3′ trailer cleavage activities of ELAC1 and ELAC2 for CCA addition. 2′,3′>p removal was assayed by incubating radiolabeled ΔCCA-HDV with 100 nM TRNT1 and serial 3-fold dilutions of ELAC1 (top left panel) or ELAC2 (top right panel). For 3′ trailer processing activity (bottom panels), the same ΔCCA leucyl-tRNA sequence was transcribed with a 13-nucleotide 3′ trailer (ΔCCA-trailer). Radiolabeled ΔCCA-trailer (pre) was incubated with 100 nM TRNT1 and serial 3-fold dilutions of ELAC1 or ELAC2. The amount of FL tRNA detected by SDS-PAGE and autoradiography was quantified and plotted.

(C) Radiolabeled *in-vitro*-transcribed ΔCCA leucyl-tRNA with the indicated trailer lengths was incubated with ELAC1, ELAC2, or yeast Trz1 and analyzed by 15% TBE-urea-PAGE and autoradiography. Precursor (pre) and cleaved (ΔCCA) products are indicated.

(D) Specialization of ELAC1 and ELAC2 function in mammalian cells for tRNA repair or tRNA biosynthesis, respectively. N_{73} refers to the discriminator base. See also Figure S3.

selectively disrupting the repair pathway. Our proposed role for ELAC1 in repairing ANKZF1-cleaved tRNAs predicts that tRNA recycling intermediates lacking intact 3′CCA ends should accumulate in cells lacking ELAC1 when ribosomes stall. To test this, we treated wild-type and ELAC1 knockout cells with the translation elongation inhibitor cycloheximide (CHX) to induce ribosome stalling (Shao et al., 2013). We detected unrepaired tRNAs by incubating RNA harvested from these cells with radiolabeled CTP and TRNT1 in the presence or absence of ELAC1 (Figure 4A). Unrepaired tRNAs should only incorporate radiolabeled CTP in the presence of ELAC1.

To control for possible global effects of CHX treatment, we calculated the ratio of radiolabeling of tRNAs extracted from CHX-treated to that of untreated cells for each cell line and

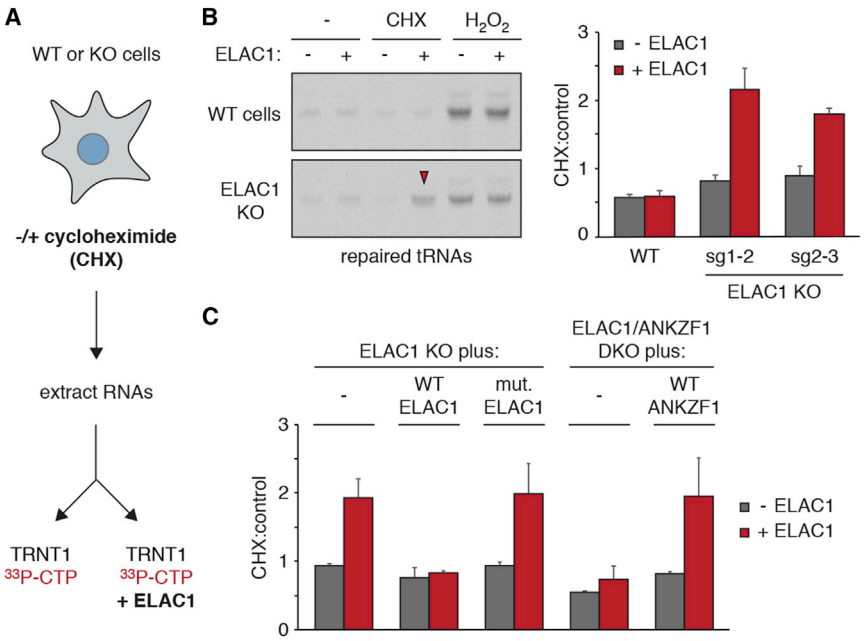

Figure 4. ELAC1 Recycles ANKZF1-Cleaved tRNAs in Cells

(A) Scheme for radiolabeling tRNA repair intermediates.

(B) WT or ELAC1 KO HEK293T cells were treated without or with 50 μg/mL cycloheximide (CHX) to induce RQC or with 2 mM H_2O_2. Total RNA extracted from these cells was incubated with 100 nM TRNT1 and 0.2 mM [α-^{33}P]-CTP without or with 20 nM ELAC1 as indicated. Re-addition of radiolabeled CTP to endogenous tRNAs was assayed by 10% TBE-urea-PAGE and autoradiography (left). Ratios of tRNA labeling from CHX-treated to untreated samples were quantified by phosphorimaging (background-subtracted values for lane 3 divided by lane 1 or for lane 4 divided by lane 2). Shown are mean values ± SEM of WT and two ELAC1 KO cell lines (right). The experiment was repeated three times.

(C) ELAC1 KO or ELAC1/ANKZF1 double-KO (DKO) HEK293T cells re-expressing nothing, WT ELAC1 or ANKZF1, or enzymatically inactive H64A ELAC1 were treated and processed as in (A) and analyzed by SDS-PAGE and autoradiography. Mean values of the ratios of tRNA labeling from CHX-treated to untreated samples ± SD for replicates of the experiment conducted in two different KO or DKO cell lines are shown.

experimental condition (Figure 4B). Comparing the same ratios from wild-type and ELAC1 knockout cells showed that the latter specifically accumulated ELAC1-dependent tRNA recycling intermediates after CHX treatment. Unrepaired tRNA levels also increased in ELAC1 knockout cells expressing a nonstop poly(A) reporter, which causes ribosome stalling independently of CHX (Juszkiewicz and Hegde, 2017; Figure S4A). This observation further supports a model in which ELAC1 acts directly downstream of ribosome stalling and verifies that the accumulation of these tRNA intermediates is not an indirect effect of global translation repression. We obtained similar results by using T4 PNK instead of ELAC1 in the labeling experiment (Figure S4B) but observed no difference in CTP labeling between wild-type and ELAC1 knockout cells treated with hydrogen peroxide, which damages the 3′ end of tRNAs independently of ribosome stalling and does not leave 2′,3′>p ends (Czech et al., 2013; Figure 4B, lanes 5 and 6).

Re-expressing wild-type ELAC1 but not catalytically inactive ELAC1(H64A) rescued tRNA recycling in ELAC1 knockout cells (Figure 4C; Figure S4C). Double-knockout cells lacking both ELAC1 and ANKZF1 did not accumulate tRNA intermediates after CHX treatment (Figure 4C; Figure S4D), supporting the idea that ANKZF1 generates these stalling-dependent tRNA intermediates upstream of ELAC1. The accumulation of intermediates was restored by re-expressing ANKZF1 in the double-knockout cells. Considered together, these results indicate that ELAC1 mediates a limiting step of recycling tRNAs cleaved by ANKZF1.

DISCUSSION

We have identified ELAC1 as a 2′,3′-cyclic phosphatase that repairs tRNAs cleaved by ANKZF1 for CCA re-addition in mammalian cells. Deleting ELAC1 leads to the ANKZF1-dependent accumulation of unrepaired tRNA intermediates specifically when ribosomes stall (Figure 4), demonstrating that both stalling-dependent tRNA cleavage and recycling occurs in cells. Because TRNT1 not only mediates CCA addition but also tags unstable tRNA structures for degradation (Wilusz et al., 2011), this recycling mechanism also mediates quality control of ANKZF1-cleaved tRNAs. These observations suggest that cells systematically check every component of stalled ribosomal complexes. Although the substrates (mRNAs) and products (nascent proteins) of aberrant translation are pre-emptively degraded (Joazeiro, 2019; Shoemaker and Green, 2012), our work reveals that peptidyl-tRNAs on stalled ribosomes are specifically processed to ensure that only functional tRNAs are re-used.

Like other RNase Z enzymes, ELAC1 binds tRNA substrates to position the ribose of the discriminator base N_{73} in its active site (Vogel et al., 2005). This mechanism is primarily used to remove 3′ trailers from tRNA precursors during tRNA biogenesis, but our findings reveal that mammalian ELAC1 has specialized in several ways to efficiently repair tRNAs. First, relative to ELAC2, ELAC1 completely converts 2′,3′>p to 2′-OH and 3′-OH on ANKZF1-cleaved tRNAs (Figures 1 and 2). ELAC1 can break both 2′ and 3′ phosphoester bonds on the ribose of N_{73}, whereas removing 3′ trailers requires hydrolyzing only the 3′ phosphoester bond. These activities are similar to bacterial CCA repair mechanisms (Yakunin et al., 2004). Second, ELAC1 has lost the ability to remove lengths of 3′ trailers typical of precursor tRNAs (Figure 3). Considered together with the localization of ELAC2 in nuclei and mitochondria and ELAC1 in the cytosol, mammalian cells appear to cleanly delegate tRNA biosynthesis and repair between the two ELAC isoforms.

Cytosolic ELAC1 can immediately repair ANKZF1-cleaved tRNAs without the need for transport back to biosynthetic sites, which may be especially advantageous for mammalian cells that are 10–100 times larger than yeast. Although a clear role for ELAC1 in repairing tRNAs released by the RQC pathway has been demonstrated, the consequences of elevated levels of non-repaired tRNAs for cellular physiology remain to be explored. Unresolved intermediates may inappropriately sequester translational factors or be further processed to tRNA fragments. ELAC1 also may be a multipurpose tRNA repair enzyme due to its versatile ability to convert different N_{73} ribose chemistries and cleave a few nucleotides from N_{73}. In addition to repairing ANKZF1-cleaved tRNAs, ELAC1 may act on nonfunctional tRNAs or tRNA-like structures with terminal phosphates or short trailers generated by damaging agents or incorrect, promiscuous, or partial processing by ELAC2 or other phosphodiesterases. ELAC enzymes also may be further specialized, particularly in organisms such as *Arabidopsis thaliana* that have multiple copies of each isoform (Canino et al., 2009). Additional specialization may be required to process tRNAs encoded in different organelles, other types of RNAs, or tRNAs damaged by diverse insults.

In addition, 2′,3′>p are commonly found in mammalian cells (Schutz et al., 2010; Shigematsu et al., 2018, 2019). They are generated by all known metal-independent nucleases and present on intermediates of mRNA, rRNA, tRNA, and U6 spliceosomal RNA biogenesis (Shigematsu et al., 2018; Zinder and Lima, 2017). With a few exceptions, such as tRNA splicing, we have little understanding of how 2′,3′>p are processed. Existing hypotheses suggest that spontaneous hydrolysis or some exosome subunits, based on structural analysis, may be able to resolve 2′,3′>p for downstream processing (Lönnberg, 2011; Rao et al., 2010; Zinder and Lima, 2017; Zinder et al., 2016). However, these mechanisms remain to be demonstrated to act directly in the context of physiological pathways. Our results indicate that ELAC1 is required to efficiently resolve 2′,3′>p on ANKZF1-cleaved tRNAs and that this function is not readily compensated by a closely related enzyme such as ELAC2. Similar requirements may apply to the resolution of 2′,3′>p on other RNAs.

STAR★METHODS

Detailed methods are provided in the online version of this paper and include the following:

- KEY RESOURCES TABLE
- LEAD CONTACT AND MATERIALS AVAILABILITY
- EXPERIMENTAL MODEL AND SUBJECT DETAILS
- METHOD DETAILS
  - Constructs
  - Recombinant protein purifications
  - tRNA production
  - *In vitro* tRNA recycling and cleavage assays
  - Fractionation of rabbit reticulocyte lysate
  - Mass spectrometry analyses
  - *In vitro* tRNA repair of RQC substrates
  - Generation of knockout cell lines
  - tRNA repair by cellular lysates
  - Detection of tRNA repair intermediates in cells
- QUANTIFICATION AND STATISTICAL ANALYSIS
- DATA AND CODE AVAILABILITY

SUPPLEMENTAL INFORMATION

Supplemental Information can be found online at https://doi.org/10.1016/j.celrep.2020.01.082.

ACKNOWLEDGMENTS

We thank the Rapoport lab for the Ulp1 SUMO protease expression plasmid; A. Johnson, Y. Miao, and Y. Shao for the T7 polymerase; R. Hegde, V. Chu, and S. Sedor for comments on the manuscript; and Shao lab members for useful discussions and help generating reagents. This work was supported by Harvard Medical School, the Richard and Susan Smith Family Foundation, the Charles H. Hood Foundation, the Vallee Scholars Program, NIH GM137415 (S. Shao), and by NIH GM67945 (S.P.G.). S. Savickas' studentship was supported by NNF16OC0030670 to Dr. Ulrich auf dem Keller.

AUTHOR CONTRIBUTIONS

M.C.J.Y. and S. Shao conceived the project. M.C.J.Y. performed and analyzed experiments. S. Savickas performed mass spectrometry analysis under the supervision of S.P.G. S. Shao supervised the project. M.C.J.Y. and S. Shao wrote the paper with input from all authors.

DECLARATION OF INTERESTS

The authors declare no competing interests.

Received: September 5, 2019
Revised: December 30, 2019
Accepted: January 22, 2020
Published: February 18, 2020

REFERENCES

Aravind, L. (1999). An evolutionary classification of the metallo-beta-lactamase fold proteins. In Silico Biol *1*, 69–91.

Beausoleil, S.A., Villén, J., Gerber, S.A., Rush, J., and Gygi, S.P. (2006). A probability-based approach for high-throughput protein phosphorylation analysis and site localization. Nat. Biotechnol. *24*, 1285–1292.

Bengtson, M.H., and Joazeiro, C.A.P. (2010). Role of a ribosome-associated E3 ubiquitin ligase in protein quality control. Nature *467*, 470–473.

Brandman, O., Stewart-Ornstein, J., Wong, D., Larson, A., Williams, C.C., Li, G.-W., Zhou, S., King, D., Shen, P.S., Weibezahn, J., et al. (2012). A ribosome-bound quality control complex triggers degradation of nascent peptides and signals translation stress. Cell *151*, 1042–1054.

Brzezniak, L.K., Bijata, M., Szczesny, R.J., and Stepien, P.P. (2011). Involvement of human ELAC2 gene product in 3′ end processing of mitochondrial tRNAs. RNA Biol. *8*, 616–626.

Canino, G., Bocian, E., Barbezier, N., Echeverría, M., Forner, J., Binder, S., and Marchfelder, A. (2009). Arabidopsis encodes four tRNase Z enzymes. Plant Physiol. *150*, 1494–1502.

Choe, Y.-J., Park, S.-H., Hassemer, T., Körner, R., Vincenz-Donnelly, L., Hayer-Hartl, M., and Hartl, F.U. (2016). Failure of RQC machinery causes protein aggregation and proteotoxic stress. Nature *531*, 191–195.

Chu, J., Hong, N.A., Masuda, C.A., Jenkins, B.V., Nelms, K.A., Goodnow, C.C., Glynne, R.J., Wu, H., Masliah, E., Joazeiro, C.A.P., and Kay, S.A. (2009). A mouse forward genetics screen identifies LISTERIN as an E3 ubiquitin ligase involved in neurodegeneration. Proc. Natl. Acad. Sci. USA *106*, 2097–2103.

Cole, S.E., LaRiviere, F.J., Merrikh, C.N., and Moore, M.J. (2009). A convergence of rRNA and mRNA quality control pathways revealed by mechanistic analysis of nonfunctional rRNA decay. Mol. Cell *34*, 440–450.

Coleman, J.E. (1992). Structure and mechanism of alkaline phosphatase. Annu. Rev. Biophys. Biomol. Struct. *21*, 441–483.

Czech, A., Wende, S., Mörl, M., Pan, T., and Ignatova, Z. (2013). Reversible and rapid transfer-RNA deactivation as a mechanism of translational repression in stress. PLoS Genet. *9*, e1003767.

Defenouillère, Q., Yao, Y., Mouaikel, J., Namane, A., Galopier, A., Decourty, L., Doyen, A., Malabat, C., Saveanu, C., Jacquier, A., and Fromont-Racine, M. (2013). Cdc48-associated complex bound to 60S particles is required for the clearance of aberrant translation products. Proc. Natl. Acad. Sci. USA *110*, 5046–5051.

Dubrovsky, E.B., Dubrovskaya, V.A., Levinger, L., Schiffer, S., and Marchfelder, A. (2004). Drosophila RNase Z processes mitochondrial and nuclear pre-tRNA 3′ ends *in vivo*. Nucleic Acids Res. *32*, 255–262.

Fan, L., Wang, Z., Liu, J., Guo, W., Yan, J., and Huang, Y. (2011). A survey of green plant tRNA 3′-end processing enzyme tRNase Zs, homologs of the candidate prostate cancer susceptibility protein ELAC2. BMC Evol. Biol. *11*, 219–222.

Feng, Q., and Shao, S. (2018). In vitro reconstitution of translational arrest pathways. Methods *15*, 20–36.

Gogakos, T., Brown, M., Garzia, A., Meyer, C., Hafner, M., and Tuschl, T. (2017). Characterizing Expression and Processing of Precursor and Mature Human tRNAs by Hydro-tRNAseq and PAR-CLIP. Cell Rep. *20*, 1463–1475.

Huttlin, E.L., Jedrychowski, M.P., Elias, J.E., Goswami, T., Rad, R., Beausoleil, S.A., Villén, J., Haas, W., Sowa, M.E., and Gygi, S.P. (2010). A tissue-specific atlas of mouse protein phosphorylation and expression. Cell *143*, 1174–1189.

Izawa, T., Park, S.-H., Zhao, L., Hartl, F.U., and Neupert, W. (2017). Cytosolic Protein Vms1 Links Ribosome Quality Control to Mitochondrial and Cellular Homeostasis. Cell *171*, 890–903.e18.

Joazeiro, C.A.P. (2019). Mechanisms and functions of ribosome-associated protein quality control. Nat. Rev. Mol. Cell Biol. *20*, 368–383.

Juszkiewicz, S., and Hegde, R.S. (2017). Initiation of Quality Control during Poly(A) Translation Requires Site-Specific Ribosome Ubiquitination. Mol. Cell *65*, 743–750.e4.

Kuroha, K., Zinoviev, A., Hellen, C.U.T., and Pestova, T.V. (2018). Release of Ubiquitinated and Non-ubiquitinated Nascent Chains from Stalled Mammalian Ribosomal Complexes by ANKZF1 and Ptrh1. Mol. Cell *72*, 286–302.e8.

Labun, K., Montague, T.G., Krause, M., Torres Cleuren, Y.N., Tjeldnes, H., and Valen, E. (2019). CHOPCHOP v3: expanding the CRISPR web toolbox beyond genome editing. Nucleic Acids Res. *47*, W171–W174.

Li de la Sierra-Gallay, I., Mathy, N., Pellegrini, O., and Condon, C. (2006). Structure of the ubiquitous 3′ processing enzyme RNase Z bound to transfer RNA. Nat. Struct. Mol. Biol. *13*, 376–377.

Limoncelli, K.A., Merrikh, C.N., and Moore, M.J. (2017). *ASC1* and *RPS3*: new actors in 18S nonfunctional rRNA decay. RNA *23*, 1946–1960.

Lönnberg, H. (2011). Cleavage of RNA phosphodiester bonds by small molecular entities: a mechanistic insight. Org. Biomol. Chem. *9*, 1687–1703.

Lykke-Andersen, J., and Bennett, E.J. (2014). Protecting the proteome: Eukaryotic cotranslational quality control pathways. J. Cell Biol. *204*, 467–476.

Lyumkis, D., Oliveira dos Passos, D., Tahara, E.B., Webb, K., Bennett, E.J., Vinterbo, S., Potter, C.S., Carragher, B., and Joazeiro, C.A.P. (2014). Structural basis for translational surveillance by the large ribosomal subunit-associated protein quality control complex. Proc. Natl. Acad. Sci. USA *111*, 15981–15986.

Phizicky, E.M., and Hopper, A.K. (2010). tRNA biology charges to the front. Genes Dev. *24*, 1832–1860.

Raasakka, A., and Kursula, P. (2014). The myelin membrane-associated enzyme 2′,3′-cyclic nucleotide 3′-phosphodiesterase: on a highway to structure and function. Neurosci. Bull. *30*, 956–966.

Ran, F.A., Hsu, P.D., Wright, J., Agarwala, V., Scott, D.A., and Zhang, F. (2013). Genome engineering using the CRISPR-Cas9 system. Nat. Protoc. *8*, 2281–2308.

Rao, F., Qi, Y., Murugan, E., Pasunooti, S., and Ji, Q. (2010). 2′,3′-cAMP hydrolysis by metal-dependent phosphodiesterases containing DHH, EAL, and HD domains is non-specific: Implications for PDE screening. Biochem. Biophys. Res. Commun. *398*, 500–505.

Rossmanith, W. (2011). Localization of human RNase Z isoforms: dual nuclear/mitochondrial targeting of the ELAC2 gene product by alternative translation initiation. PLoS One *6*, e19152.

Schürer, H., Lang, K., Schuster, J., and Mörl, M. (2002). A universal method to produce *in vitro* transcripts with homogeneous 3′ ends. Nucleic Acids Res. *30*, e56.

Schutz, K., Hesselberth, J.R., and Fields, S. (2010). Capture and sequence analysis of RNAs with terminal 2′,3′-cyclic phosphates. RNA *16*, 621–631.

Shao, S., and Hegde, R.S. (2014). Reconstitution of a minimal ribosome-associated ubiquitination pathway with purified factors. Mol. Cell *55*, 880–890.

Shao, S., von der Malsburg, K., and Hegde, R.S. (2013). Listerin-dependent nascent protein ubiquitination relies on ribosome subunit dissociation. Mol. Cell *50*, 637–648.

Shao, S., Brown, A., Santhanam, B., and Hegde, R.S. (2015). Structure and assembly pathway of the ribosome quality control complex. Mol. Cell *57*, 433–444.

Shen, P.S., Park, J., Qin, Y., Li, X., Parsawar, K., Larson, M.H., Cox, J., Cheng, Y., Lambowitz, A.M., Weissman, J.S., et al. (2015). Protein synthesis. Rqc2p and 60S ribosomal subunits mediate mRNA-independent elongation of nascent chains. Science *347*, 75–78.

Shigematsu, M., Kawamura, T., and Kirino, Y. (2018). Generation of 2′,3′-Cyclic Phosphate-Containing RNAs as a Hidden Layer of the Transcriptome. Front. Genet. *9*, 562.

Shigematsu, M., Morichika, K., Kawamura, T., Honda, S., and Kirino, Y. (2019). Genome-wide identification of short 2′,3′-cyclic phosphate-containing RNAs and their regulation in aging. PLoS Genet. *15*, e1008469.

Shoemaker, C.J., and Green, R. (2012). Translation drives mRNA quality control. Nat. Struct. Mol. Biol. *19*, 594–601.

Shoemaker, C.J., Eyler, D.E., and Green, R. (2010). Dom34:Hbs1 promotes subunit dissociation and peptidyl-tRNA drop-off to initiate no-go decay. Science *330*, 369–372.

Siira, S.J., Rossetti, G., Richman, T.R., Perks, K., Ermer, J.A., Kuznetsova, I., Hughes, L., Shearwood, A.J., Viola, H.M., Hool, L.C., et al. (2018). Concerted regulation of mitochondrial and nuclear non-coding RNAs by a dual-targeted RNase Z. EMBO Rep. *19*, e46198.

Sugiyama, T., Li, S., Kato, M., Ikeuchi, K., Ichimura, A., Matsuo, Y., and Inada, T. (2019). Sequential Ubiquitination of Ribosomal Protein uS3 Triggers the Degradation of Non-functional 18S rRNA. Cell Rep. *26*, 3400–3415.e7.

Takahashi, M., Takaku, H., and Nashimoto, M. (2008). Regulation of the human tRNase ZS gene expression. FEBS Lett. *582*, 2532–2536.

Takaku, H., Minagawa, A., Takagi, M., and Nashimoto, M. (2003). A candidate prostate cancer susceptibility gene encodes tRNA 3′ processing endoribonuclease. Nucleic Acids Res. *31*, 2272–2278.

Tavtigian, S.V., Simard, J., Teng, D.H., Abtin, V., Baumgard, M., Beck, A., Camp, N.J., Carillo, A.R., Chen, Y., Dayananth, P., et al. (2001). A candidate prostate cancer susceptibility gene at chromosome 17p. Nat. Genet. *27*, 172–180.

Verma, R., Oania, R.S., Kolawa, N.J., and Deshaies, R.J. (2013). Cdc48/p97 promotes degradation of aberrant nascent polypeptides bound to the ribosome. eLife *2*, e00308.

Verma, R., Reichermeier, K.M., Burroughs, A.M., Oania, R.S., Reitsma, J.M., Aravind, L., and Deshaies, R.J. (2018). Vms1 and ANKZF1 peptidyl-tRNA hydrolases release nascent chains from stalled ribosomes. Nature *557*, 446–451.

Vogel, A., Schilling, O., Späth, B., and Marchfelder, A. (2005). The tRNase Z family of proteins: physiological functions, substrate specificity and structural properties. Biol. Chem. *386*, 1253–1264.

Wang, Z., Zheng, J., Zhang, X., Peng, J., Liu, J., and Huang, Y. (2012). Identification and sequence analysis of metazoan tRNA 3′-end processing enzymes tRNase Zs. PLoS One *7*, e44264.

Wilusz, J.E., Whipple, J.M., Phizicky, E.M., and Sharp, P.A. (2011). tRNAs marked with CCACCA are targeted for degradation. Science *334*, 817–821.

Yakunin, A.F., Proudfoot, M., Kuznetsova, E., Savchenko, A., Brown, G., Arrowsmith, C.H., and Edwards, A.M. (2004). The HD domain of the Escherichia coli tRNA nucleotidyltransferase has 2′,3′-cyclic phosphodiesterase, 2′-nucleotidase, and phosphatase activities. J. Biol. Chem. *279*, 36819–36827.

Yan, H., Zareen, N., and Levinger, L. (2006). Naturally occurring mutations in human mitochondrial pre-tRNASer(UCN) can affect the transfer ribonuclease Z cleavage site, processing kinetics, and substrate secondary structure. J. Biol. Chem. *281*, 3926–3935.

Yip, M.C.J., Keszei, A.F.A., Feng, Q., Chu, V., McKenna, M.J., and Shao, S. (2019). Mechanism for recycling tRNAs on stalled ribosomes. Nat. Struct. Mol. Biol. *26*, 343–349.

Zinder, J.C., and Lima, C.D. (2017). Targeting RNA for processing or destruction by the eukaryotic RNA exosome and its cofactors. Genes Dev. *31*, 88–100.

Zinder, J.C., Wasmuth, E.V., and Lima, C.D. (2016). Nuclear RNA Exosome at 3.1 Å Reveals Substrate Specificities, RNA Paths, and Allosteric Inhibition of Rrp44/Dis3. Mol. Cell *64*, 734–745.

Zurita Rendón, O., Fredrickson, E.K., Howard, C.J., Van Vranken, J., Fogarty, S., Tolley, N.D., Kalia, R., Osuna, B.A., Shen, P.S., Hill, C.P., et al. (2018). Vms1p is a release factor for the ribosome-associated quality control complex. Nat. Commun. *9*, 2197.

STAR★METHODS

KEY RESOURCES TABLE

REAGENT or RESOURCE	SOURCE	IDENTIFIER
Antibodies		
Monoclonal mouse anti-ELAC1	Santa Cruz	Cat#sc-390029
Polyclonal rabbit anti-TRNT1	Novus Biologicals	Cat#NBP1-86589; RRID: AB_11016077
Polyclonal rabbit anti-ELAC2	Bethyl Laboratories	Cat#A304-775A; RRID: AB_2620970
Monoclonal mouse anti-ANKZF1	Santa Cruz	Cat#sc-398713
Monoclonal mouse anti-Flag M2	Sigma	Cat#3165; RRID: AB_259529
Polyclonal rabbit anti-GFP	homemade	N/A
Polyclonal rabbit anti-RFP	homemade	N/A
Monoclonal rabbit anti-uL2	Abcam	Cat#ab169538; RRID: AB_2714187
HRP-conjugated goat anti-rabbit	Jackson ImmunoResearch	Cat#111-035-003; RRID: AB_2313567
HRP conjugated goat anti-mouse	Jackson ImmunoResearch	Cat#115-035-003; RRID:AB_10015289
Bacterial and Virus Strains		
BL21 (DE3) competent cells	Invitrogen	Cat#C600003
DH5α competent cells	Invitrogen	Cat#18265017
Rosetta2 (DE3) competent cells	Millipore	Cat#71400
Chemicals, Peptides, and Recombinant Proteins		
TRNT1	Yip et al., 2019	N/A
ELAC1	This study	N/A
ELAC1 (H64A)	This study	N/A
ELAC2 (31-826)	This study	N/A
ELAC2 (31-826, H548A)	This study	N/A
Trz1p	This study	N/A
Vms1p	Yip et al., 2019	N/A
DN-Hbs1L	Shao et al., 2013	N/A
Hbs1L	Shao and Hegde, 2014	N/A
Pelota	Shao and Hegde, 2014	N/A
ABCE1	Shao and Hegde, 2014	N/A
NEMF	Shao et al., 2015	N/A
RtcB	New England Biolabs	Cat#M0458
CNP	This study	N/A
T4 PNK	New England Biolabs	Cat#M0201
T7 RNA polymerase	homemade	N/A
Creatine phosphate	Roche	Cat#621714
Creatine kinase	Roche	Cat#127566
SuperTEV	homemade	N/A
Ulp1 SUMO protease	homemade	N/A
3C protease	homemade	N/A
Ni-NTA agarose	QIAGEN	Cat#30250
Glutathione Sepharose 4B	GE Healthcare	Cat#17-0756
DEAE Sepharose Fast Flow	GE Healthcare	Cat#17-0709
Phenyl Sepharose 6 Fast Flow	GE Healthcare	Cat#17-0973
HiTrap Heparin HP affinity column	GE Healthcare	Cat#17040601
L-Glutathione reduced	Sigma	Cat#G4251
Cycloheximide	CalBiochem	Cat#239763

(*Continued on next page*)

Continued		
REAGENT or RESOURCE	SOURCE	IDENTIFIER
Puromycin dihydrochloride	GIBCO	Cat#A1113803
[α-^{33}P]-CTP	American Radiolabeled Chemicals	Cat#ARP0154
TRI Reagent	Zymo Research	Cat#R2050-1
rRnasin	Promega	Cat#N2511
Complete EDTA-free protease inhibitor cocktail	Roche	Cat#11873580001
TransIT 293	Mirus	Cat#MIR2706
SYBR Gold	Invitrogen	Cat#S11494
Hydrogen peroxide	Sigma	Cat#216763
S. cerevisiae genomic DNA	Novagen	Cat#69240-3
M2 Flag affinity resin	Sigma	Cat#A2220
3x Flag peptide	Sigma	Cat#F4799
Rabbit reticulocyte translation system	Feng and Shao, 2018	N/A
Experimental Models: Cell Lines		
HEK293T	ATCC	Cat#CRL-11268
ELAC1 KO sg1-2 293T	This study	N/A
ELAC1 KO sg1-5 293T	This study	N/A
ELAC1 KO sg2-3 293T	This study	N/A
ELAC1 KO sg2-9 293T	This study	N/A
ANKZF1 KO sg1-3 293T	This study	N/A
ELAC1/ANKZF1 DKO sg1-1 293T	This study	N/A
ELAC1/ANKZF1 DKO sg1-2 293T	This study	N/A
Oligonucleotides		
ELAC1 sg2 TAAAGTCCCGAAGCCCTACA	This study	N/A
ELAC1 sg1 AGCACTCGCCTTCACACCGA	This study	N/A
ANKZF1 sg1 GCTTGGCCCGAACCGTATAG	This study	N/A
Recombinant DNA		
pRSETA-TRNT1	Yip et al., 2019	N/A
pGEX-ELAC1	This study	N/A
pGEX-ELAC1 (H64A)	This study	N/A
pK27SUMO-ELAC2 (31-826)	This study	N/A
pK27SUMO-ELAC2 (31-826, H548A)	This study	N/A
pK27SUMO-Trz1	This study	N/A
pLeuUUA-HDV-ΔCCA	Yip et al., 2019	N/A
pX459-sgELAC1-1	This study	N/A
pX459-sgELAC1-2	This study	N/A
pRSETA-CNP	This study	N/A
pSP64-3XFlag-VHP68	Shao et al., 2013	N/A
pX459-sgANKZF1-1	This study	N/A
pcDNA3.1-3XFlag-ELAC1	This study	N/A
pcDNA3.1-3XFlag-ELAC1 (H64A)	This study	N/A
pcDNA3.1-3XFlag-ANKZF1	Yip et al., 2019	N/A
pcDNA5-FRT/TO-GFP-P2A-repA0-P2A-RFP	Juszkiewicz and Hegde, 2017	N/A
pcDNA5-FRT/TO-GFP-P2A-repA63-P2A-RFP	Juszkiewicz and Hegde, 2017	N/A

LEAD CONTACT AND MATERIALS AVAILABILITY

Request for reagents may be directed to Lead Contact Sichen Shao (sichen_shao@hms.harvard.edu). Plasmids generated in this study are available from the Lead Contact without restriction. All other unique/stable reagents generated in this study will be made available on request but may require a completed Materials Transfer Agreement.

EXPERIMENTAL MODEL AND SUBJECT DETAILS

HEK293T cells authenticated by STR profiling were cultured in Dulbecco's Modified Eagle's Medium (DMEM) with 10% fetal calf serum (FCS) at 37°C and 5% CO_2.

METHOD DETAILS

Constructs

TRNT1 (HsCD00329081), ELAC1 (HsCD00322240), ELAC2 (HsCD00321566), and CNP (HsCD00336380) cDNA was obtained from the PlasmID repository at Harvard Medical School. Trz1 was cloned from *S. cerevisiae* genomic DNA (Novagen). Mammalian and bacterial expression plasmids encoding wild-type and dominant negative Hbs1L, Pelota, ABCE1, NEMF, and Vms1, as well as an SP64 vector for *in vitro* transcription and translation of a stalling reporter, are as previously described (Shao et al., 2013, 2015; Shao and Hegde, 2014; Yip et al., 2019). The open reading frames of TRNT1 and CNP were cloned into a pRSETA expression vector encoding an N-terminal His-TEV tag; the open reading frame of ELAC1 was cloned into a pGEX bacterial expression vector encoding an N-terminal GST-3C tag, as well as a pcDNA3.1 mammalian expression vector behind an N-terminal 3X Flag tag; ELAC2 and Trz1 were cloned into a pRSETA vector containing an N-terminal His-SUMO tag. The first 30 residues of ELAC2 containing the mitochondrial targeting sequence were removed. Point mutations were made using Phusion (NEB) mutagenesis according to the manufacturer's instructions.

Recombinant protein purifications

TRNT1, ELAC1, ELAC2, Trz1, and CNP were expressed and purified using standard procedures. TRNT1 and CNP were expressed in BL21 (DE3) cells, while ELAC1, ELAC2 and Trz1 were expressed in Rosetta 2 cells. Transformed cells were grown to an OD_{600} of 0.6-0.8 in LB under the appropriate antibiotic selection, then induced with 0.2 mM IPTG at 16°C overnight. Cells were harvested by centrifugation and resuspended in lysis buffer (1x PBS, 250 mM NaCl, 1 mM DTT, 1x protease inhibitor cocktail for His-tagged proteins, or 1x PBS, 1 mM DTT, 1x protease inhibitor cocktail for GST-tagged proteins). The cells were lysed by two applications through a microfluidizer. Lysates were clarified by centrifugation, and the supernatant passed over 1 mL of NiNTA resin or GST resin equilibrated in lysis buffer. The resin was then washed with 10 column volumes of lysis buffer. For ELAC1, ELAC2, and Trz1, the resin was also washed with lysis buffer supplemented with 1 M NaCl to remove RNA contamination.

The proteins were eluted with elution buffer (1x PBS, 250 mM NaCl, 200 mM imidazole, 1 mM DTT for His-TEV-tagged proteins, or 1x PBS, 250 mM NaCl, 400 mM imidazole, 1 mM DTT for His-SUMO-tagged proteins, or 50 mM Tris pH 8, 25 mM glutathione for GST-tagged proteins). Peak fractions were pooled and dialyzed in 50 mM HEPES pH 7.5, 100 mM KOAc, 2.5 mM $Mg(OAc)_2$, 10% glycerol, 1 mM DTT, and for His-tagged proteins, 10 mM imidazole, overnight in the presence of SuperTEV, SUMO protease (Ulp1), or 3C protease for His-TEV-tagged, His-SUMO-tagged, and GST-tagged proteins respectively. Cleaved tags and protease were subtracted, and the purified proteins were pooled, aliquoted, frozen in liquid nitrogen, and stored at −80°C.

tRNA production

tRNA sequences were transcribed from PCR-amplified templates as previously stated (Yip et al., 2019). Templates were generated from PCR amplifications of plasmid-borne DNA sequences of $tRNA^{Leu(UAA)}$ or ΔCCA-HDV using forward primers containing a T7 promoter and reverse primers generating the appropriate 3′ end. Transcription reactions contained 60 mM HEPES pH 7.5, 25 mM NaCl, 18 mM $MgCl_2$, 2 mM spermidine, 10 mM DTT, 0.5 mM NTPs, 0.2U/μL recombinant RNasin (Promega), and 21 μg/mL T7 polymerase. Where applicable, [α-^{33}P]-CTP was added at a 1:1 ratio to unlabeled CTP (0.25 mM each). Reactions were incubated at 37°C for 4 h, stopped with the addition of three volumes of Trizol, and the tRNAs purified using Directzol columns (Zymo Research).

In vitro tRNA recycling and cleavage assays

In vitro tRNA repair reactions were performed in PSB (50 mM HEPES pH 7.5, 100 mM KOAc, 2.5 mM $Mg(OAc)_2$, 1 mM DTT) with 0.5 mM NTPs, 10 μg/mL creatine kinase, 6 mM creatine phosphate, 100 nM TRNT1, 2 ng/μL radiolabeled ΔCCA-HDV transcripts and where applicable, 100 nM ELAC1, 40 U/mL CIP (NEB) or 0.375 U/μL T4 PNK. Unless indicated otherwise, reactions were at 32°C for 30 min, quenched with sample buffer (50 mM Tris pH 6.8, 1% SDS, 10% glycerol, 100 mM DTT), and analyzed by SDS-PAGE and autoradiography.

RtcB reactions were performed with 20 ng/μL of radiolabeled ΔCCA-HDV, 0.1 mM GTP, and 0.75 μM RtcB (NEB) in the supplied buffer (50 mM Tris-HCl pH 8.3, 75 mM KCl, 3 mM $MgCl_2$, 10 mM DTT). CNP reactions were performed with 20 ng/μL of radiolabeled ΔCCA-HDV and 100 nM recombinant CNP in PSB (50 mM HEPES pH 7.5, 100 mM KOAc, 2.5 mM $Mg(OAc)_2$, 1 mM DTT). Reactions were incubated at 37°C for 1 h, stopped with addition of three volumes of Trizol, and the tRNA re-extracted using Directzol columns (Zymo Research) and used for repair reactions as described above.

Fractionation of rabbit reticulocyte lysate

Rabbit reticulocyte lysate was centrifuged in a TLA100.3 rotor at 100,000 rpm for 40 min. The supernatant was diluted in an equal volume of column buffer (20 mM Tris pH 7.5, 20 mM KCl, 0.1 mM EDTA, 10% glycerol, 1 mM DTT) and applied over 10 mL

of equilibrated DEAE Sepharose resin. The resin was washed with 16 mL column buffer, and stepwise elutions were collected with column buffer containing 50 mM, 100 mM, 150 mM or 250 mM KCl. The 100 mM elution containing peak phosphatase activity was then incubated with 8 mL phenyl Sepharose resin for 1 h at 4°C. The flow-through was collected and elution was carried out with 15 mL column buffer containing 1% Triton X-100. The phenyl Sepharose flow-through was then loaded onto a HiTrap Heparin HP column (GE Healthcare Life Sciences) equilibrated in buffer A (20 mM Tris pH 7.5, 100 mM KCl, 5 mM $Mg(OAc)_2$, 10% glycerol, 1 mM DTT), washed with 3 mL of buffer A, and eluted into 30 column volumes of buffer B (10 mM $NaPO_4$ pH 7, 1 M NaCl, 5 mM $Mg(OAc)_2$, 10% glycerol, 1 mM DTT), collecting 1 mL fractions. Fractions 9 and 10 containing peak activity were pooled, concentrated with a Vivaspin-2 (3000 MWCO) concentrator and loaded onto a Superdex200 10/300 increase column equilibrated with SEC buffer (50 mM HEPES pH 7.5, 100 mM KOAc, 2.5 mM $Mg(OAc)_2$, 10% glycerol, 1 mM DTT).

To test for repair activity, 500 μL of each fraction was exchanged into 1 mL PSB (50 mM HEPES pH 7.5, 100 mM KOAc, 2.5 mM $Mg(OAc)_2$) using a PD MiniTrap G-25 column (GE Healthcare Life Sciences). 8 μL of each fraction was used in 10 μL *in vitro* recycling reactions of radiolabeled ΔCCA-HDV transcripts containing 100 nM TRNT1 as described above.

Mass spectrometry analyses

Lysate fractions were concentrated by TCA precipitation and resuspended in 8 M urea in 200 mM EPPS, pH 8.5. Room temperature samples were subject to reduction with 5 mM tris(2-carboxyethyl)phosphine for 15 min, alkylation with 10 mM iodoacetamide for 30 min in the dark, and quenched with 10 mM DTT for 15 min. After the addition of 8x sample volume of 200 mM EPPS, pH 8.5, the sample was digested with 100 ng of trypsin overnight at 37°C. Trypsinized samples were adjusted to 1% TFA, desalted over a StageTip containing Empore C18 with 12-16 μg peptide capacity, eluted in 80% Acetonitrile, 0.1% TFA, dried in a SpeedVac, and resuspended in LC-MS buffer (5% Acetonitrile, 5% Formic acid). Mass spectrometry data were collected using a Q Exactive mass spectrometer (ThermoFisher Scientific, San Jose, CA) coupled to a Proxeon EASY-nLC 1200 liquid chromatography (LC) pump (Thermo Fisher Scientific). Peptides were separated for 150 min on a 100 μm inner diameter microcapillary column packed with Accucore C18 resin (2.6μm, 150Å, ThermoFisher). For analysis, ~1μg was loaded onto the analytical column. An in-house database search engine included all entries of *Oryctolagus cuniculus* from the UniProt Database (December 10, 2018). The database was concatenated with one composed of all protein sequences in reversed order. We applied 50 ppm precursor ion tolerance for total protein level identification and 0.03 for fragment ion tolerance. The tolerance windows were chosen together with SEQUEST searches and linear discriminant analysis (Beausoleil et al., 2006; Huttlin et al., 2010). Carbamidomethylation of cysteine residues (+57.021 Da) was set as a static modification, while Oxidation (+15.995 Da) was set as a variable modification. Peptide-spectrum matches (PSM's) did not exceed 1% false discovery rate (FDR). Linear discriminant analysis was used for PSM filtering as described previously (Huttlin et al., 2010). Filtered PSM's were further filtered for protein-level FDR of 1%.

In vitro tRNA repair of RQC substrates

In vitro transcription, translation, and purification of stalled ribosome-nascent protein complexes were performed as previously described (Shao and Hegde, 2014). Briefly, mRNAs were transcribed from SP6 promoter constructs encoding a 3X Flag tag, the autonomously folding villin headpiece domain, and the unstructured cytosolic region of Sec61β truncated at valine 68 (Shao et al., 2013). Translation reactions in rabbit reticulocyte lysate were at 32°C for 20 min. 50 μM of purified GTPase deficient Hbs1L was added 7 min into the translation reaction. Reactions were adjusted to 750 mM KOAc and centrifuged at 100,000 rpm for 1 h over a 0.5 M sucrose cushion in 50 mM HEPES, pH 7.4, 750 mM KOAc, 15 mM $Mg(OAc)_2$ at 4°C in a TLA100.3 rotor (Beckman Coulter). Pelleted ribosomes were resuspended in RNC buffer (50 mM HEPES, pH 7.4, 100 mM KOAc, 5 mM $Mg(OAc)_2$, 1 mM DTT) and incubated with M2 Flag resin for 1 h at 4°C. The resin was washed sequentially with 6 mL RNC buffer with 0.1% Triton X-100, 6 mL 50 mM HEPES, pH 7.4, 250 mM KOAc, 5 mM $Mg(OAc)_2$, 0.5% Triton X-100, 1 mM DTT, and 6 mL RNC buffer, and eluted with 0.1 mg/mL 3X Flag peptide in RNC buffer at room temperature for 25 min. Purified RNCs were directly incubated with an energy regenerating system and purified ribosome splitting factors (50 nM Hbs1L, 50 nM Pelota, 100 nM ABCE1), 10 nM NEMF, 125 nM Vms1, without or with 100 nM wild-type or H64A ELAC1, 100 nM TRNT1, 0.375 U/μL T4 PNK, and 0.2 mM [α-^{33}P]-CTP for 20 min at 32°C. NC-tRNAs were deacylated by the addition of 37.5 mM NaOH and incubated on ice for 5 min before RNAs were isolated using Directzol columns and directly analyzed by TBE-urea-PAGE and autoradiography.

Generation of knockout cell lines

Guide RNAs for CRISPR were designed using ChopChop v3 (Labun et al., 2019) and inserted into pX459 (Ran et al., 2013). 500 ng of pX459 containing individual guide RNAs was transfected into HEK293T cells in a 6-well plate using TransIT293 (Mirus) according to the manufacturer's instructions. After 24 h, the cells were placed under 2 μg/mL puromycin selection for 48 h. Single clones were isolated and knockouts were confirmed by immunoblotting and mutations validated by amplicon sequencing.

tRNA repair by cellular lysates

Wild-type or ELAC1 knockout HEK293T cells were washed, harvested, and pelleted in cold PBS. Cells were incubated in an equal volume of hypotonic lysis buffer (10 mM HEPES pH 7.5, 10 mM KOAc, 1.5 mM $Mg(OAc)_2$, 1 mM DTT, 1x protease inhibitor cocktail) for 30 min on ice before being lysed through a 26 Gauge needle. Lysates were adjusted to 90 mM KOAc, clarified by centrifugation, and directly used for subsequent reactions. Where applicable, knockdowns of TRNT1 were for 72 h as previously described

(Yip et al., 2019) using Lipofectamine RNAiMAX (Life Technologies) according to the manufacturer's instructions before processing. tRNA repair reactions were performed as above with 20 ng/μL ΔCCA-HDV and 10.9 mg/mL lysate at 37°C for 30 min, quenched with three volumes of Trizol, and isolated RNA was analyzed by TBE-urea-PAGE and autoradiography.

Detection of tRNA repair intermediates in cells

Wild-type or knockout HEK293T cells were treated at 50%–70% confluency with 50 μg/mL cycloheximide for 30 min at 37°C. Cells were washed, harvested, and pelleted in cold PBS containing 5 μg/mL cycloheximide before being lysed in an equal volume of 50 mM HEPES pH 7.5, 100 mM KOAc, 5 mM $Mg(OAc)_2$, 1 mM DTT, 0.02% digitonin, 50 μg/mL cycloheximide on ice for 10 min. Following clarification by centrifugation, RNAs were isolated using Directzol columns and directly subject to *in vitro* repair assays as described above containing 0.2 mM [α-^{33}P]-CTP at 37°C for 30 min. Isolated RNAs were analyzed by TBE-urea-PAGE or SDS-PAGE and autoradiography. Transient transfections of poly(A), Flag-tagged wild-type ELAC1, ANKZF1, or H64A ELAC1 constructs were with TransIT293 (Mirus) for 24 h according to the manufacturer's instructions. Quantification was performed from film scans in ImageJ (NIH) or by phosphorimaging and ImageQuant (GE Healthcare). Background-subtracted values were used to calculate ratios of CHX- to untreated samples without or with ELAC1 present in the labeling assay.

QUANTIFICATION AND STATISTICAL ANALYSIS

ImageJ (NIH) and ImageQuant TL 8.1 (GE Healthcare) were used to quantify band intensities for Figures 3B, 4B,4C, S3C, and S4A. For ImageJ analysis, boxes of identical sizes were drawn around the bands of interest, and the average intensity value was subtracted against the average background intensity. For ImageQuant TL 8.1 analysis, bands were automatically detected to determine the corresponding background subtracted intensity volumes. For Figures 3B and S3C, the band intensity of the modified tRNA ('FL') was normalized against the band intensity of the strongest 'FL' signal generated by the indicated enzyme in reactions containing equal amounts of starting substrates and in identical autoradiography exposure conditions. The experiment in Figure 4B was repeated three times (n = 3) with WT and two ELAC1 knockout cell lines. The ratios of tRNA labeling from CHX-treated to untreated samples (background-subtracted values for lane 3 divided by lane 1, or for lane 4 divided by lane 2) were calculated, and the mean values of these ratios plotted. Error bars denotes standard error of the mean (s.e.m.) as indicated in the figure legend. For Figure 4C, two different cell lines (n = 2) were analyzed for each condition. The ratios of tRNA labeling from CHX-treated to untreated samples were calculated, and the mean values of these ratios were plotted. Error bars denote standard deviation (s.d.) as indicated in the figure legend. For Supplemental Figure S4A, the ratios of tRNA labeling from cells expressing a control or poly(A) nonstop reporter protein (background-subtracted values for lane 3 divided by lane 1, or for lane 4 divided by lane 2) were quantified and directly reported.

DATA AND CODE AVAILABILITY

This study did not generate any unique datasets or code.

Cell Reports, Volume *30*

Supplemental Information

ELAC1 Repairs tRNAs Cleaved during Ribosome-Associated Quality Control

Matthew C.J. Yip, Simonas Savickas, Steven P. Gygi, and Sichen Shao

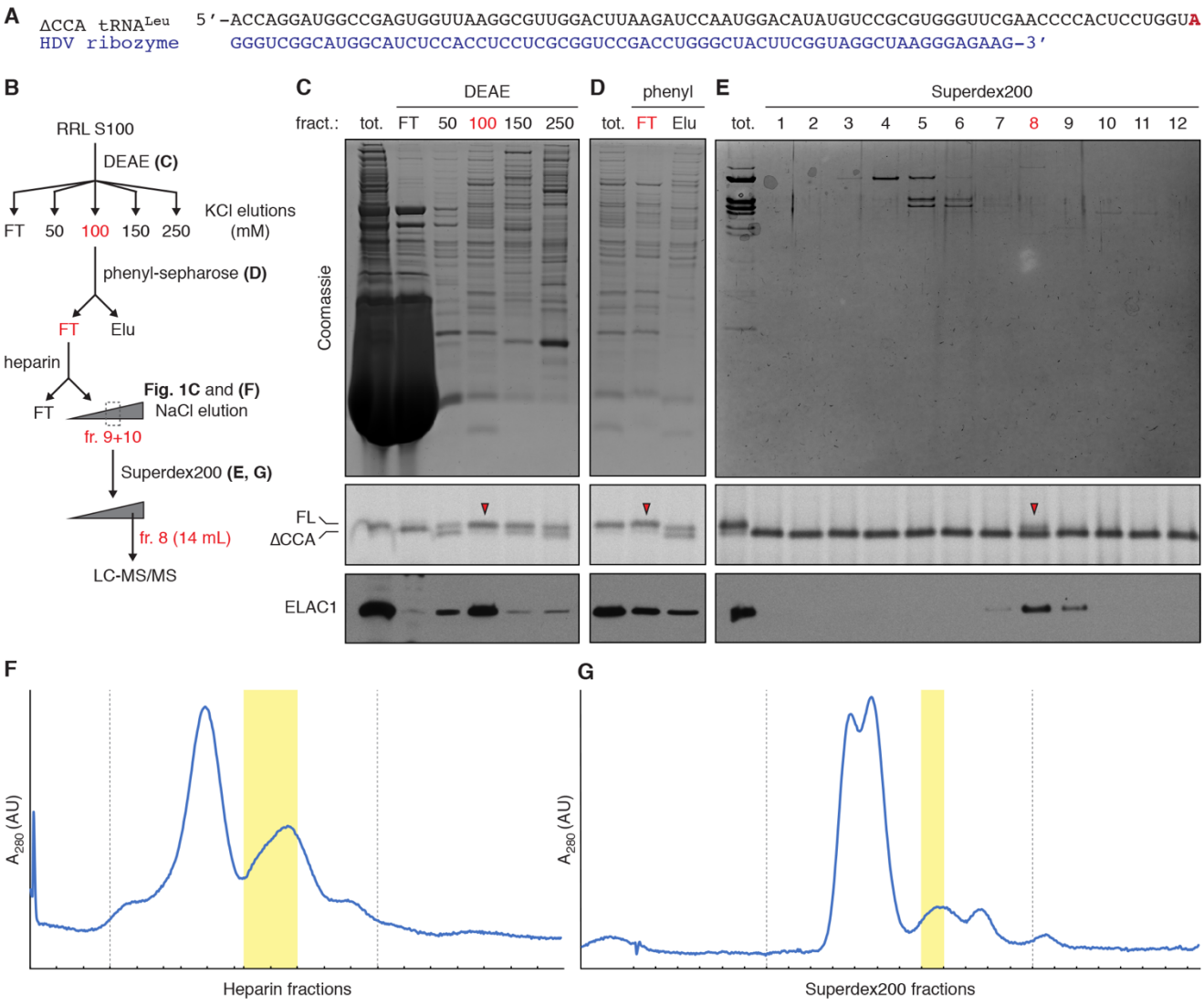

Figure S1. Identification of ELAC1 by activity-guided fractionation (related to Fig. 1). (A) Sequence of ΔCCA-HDV encoding a CCA-less leucyl tRNA (ΔCCA $tRNA^{Leu}$; black, discriminator base in red) fused to the Hepatitis Delta virus (HDV) ribozyme (blue). **(B)** Fractionation scheme of ribosome-free rabbit reticulocyte lysate (RRL S100). Fractions containing peak tRNA repair activity and carried forward in the fractionation scheme are shown in red. **(C-E)** Individual fractions at different biochemical fractionation steps depicted in **(B)** were directly analyzed by SDS-PAGE and Coomassie stain (top), incubated with 2 ng/µL radiolabeled ΔCCA-HDV and 100 nM TRNT1 to assay for CCA addition by SDS-PAGE and autoradiography (middle), or immunoblotting for ELAC1 (bottom). Fractions containing peak repair activity (red arrowheads) and carried forward in the fractionation pipeline are denoted in red. **(F)** Absorbance at 280 nm for the elution of RRL fractions from a heparin resin by a gradient of NaCl. Dotted gray lines indicate fractions analyzed in Fig. **1C**; peak repair activity was observed in the yellow fractions, which were pooled and subject to subsequent fractionation. **(G)** Absorbance at 280 nm for the final size exclusion fractionation step. Dotted gray lines indicate fractions analyzed in **(E)**; the fraction containing peak repair activity is colored yellow and was submitted for protein identification.

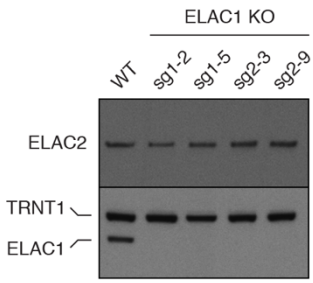

Figure S2. Generation of ELAC1 knockout cell lines (related to Fig. 2). Immunoblotting for ELAC1, ELAC2, and TRNT1 of cytosolic lysates isolated as in Fig. **2C** from wildtype (WT) and four clonal lines of ELAC1 knockout (KO) HEK293T cells generated from two different guide RNAs (sg1 and sg2; see Key Resources Table). All four ELAC1 KO cell lines were validated to be impaired in tRNA recycling using the assay shown in Fig. **2C**. Lysates displayed in Fig. **2C** and Fig. **S3C** are from sg1-5 and sg2-9. All other experiments (Fig. **4** and **S4**) were done with sg1-2 and sg2-3.

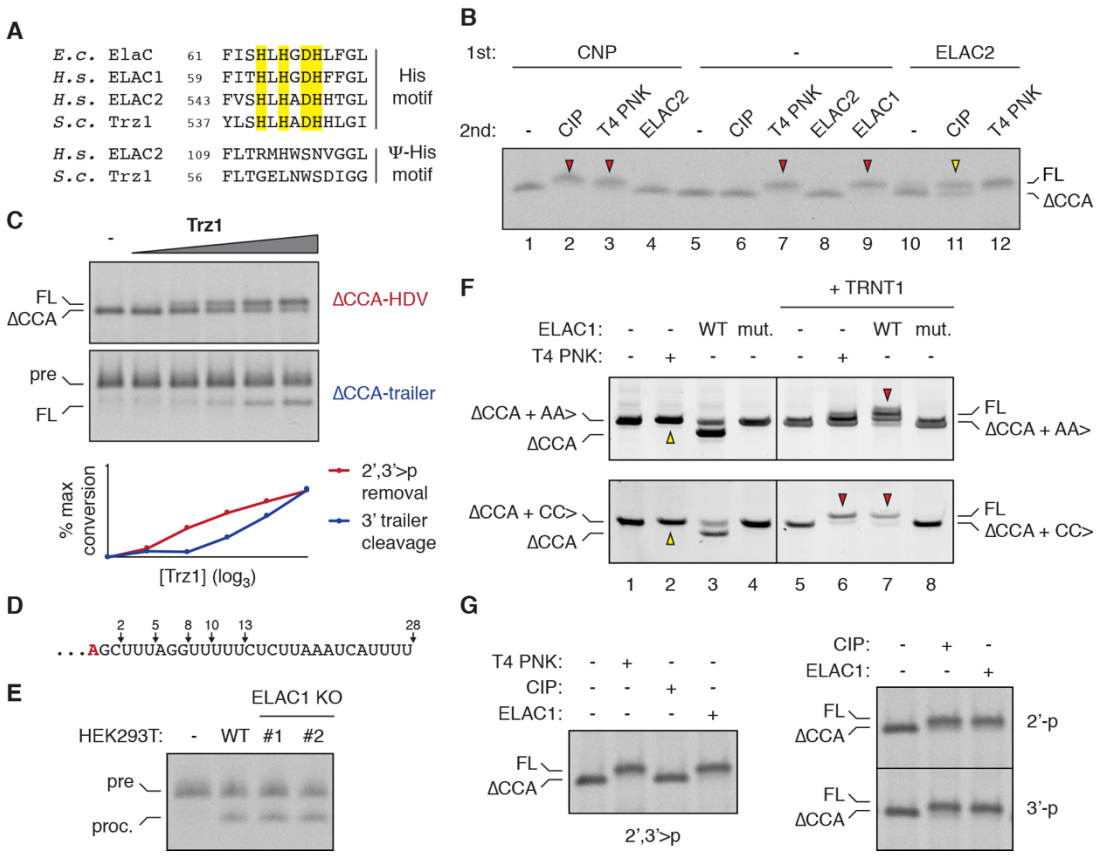

Figure S3. Specialization of eukaryotic ELAC isoforms (related to Fig. 3). (A) Alignments of catalytic His or catalytically inactive pseudo-His (Ψ-His) motifs in the indicated RNase Z isoforms from bacteria (*E.c.* ElaC), humans (*H.s.* ELAC1 and ELAC2), and yeast (*S.c.* Trz1). The catalytic HxHxDH residues are highlighted in yellow. **(B)** Radiolabeled ΔCCA-HDV was treated sequentially (1st) without or with CNP or ELAC2, followed by (2nd) TRNT1 without or with CIP, T4 PNK, ELAC1, or ELAC2. Analysis by SDS-PAGE and autoradiography revealed complete (red arrowheads) or partial (yellow arrowhead) CCA addition. **(C)** Yeast Trz1 2',3'>p removal and 3' trailer cleavage activity as in Fig. **3B**. 2',3'-cyclic phosphatase activity was assayed by incubating radiolabeled ΔCCA-HDV with 100 nM TRNT1 and serial 3-fold dilutions of Trz1. 3' trailer processing activity was assayed by incubating radiolabeled ΔCCA-trailer (pre) with 100 nM TRNT1 and serial 3-fold dilutions of Trz1. The amount of mature full-length (FL) tRNA produced in each reaction was quantified and plotted (bottom). **(D)** Genomic 3' trailer sequence of ΔCCA leucyl-tRNA following the discriminator base (red). Different lengths analyzed in Fig. **3C** are annotated. **(E)** Radiolabeled ΔCCA-trailer was incubated without or with hypotonic lysates from wildtype (WT) or ELAC1 knockout (KO) HEK293T cells (as in Fig. **2C**). Processing (proc.) of ΔCCA-trailer (pre) was assayed by SDS-PAGE and autoradiography. Note that the extent of 3' trailer cleavage does not change by removing ELAC1 activity. **(F)** Transcribed ΔCCA leucyl-tRNA with two adenine (ΔCCA + AA>; top panel) or cytidine (ΔCCA + CC>; bottom panel) nucleotides in front of a 3' HDV ribozyme to generate 2',3'>p on the ribose at position 75 was incubated with 0.375 U/μL T4 PNK or 100 nM wildtype (WT) or catalytically inactive H64A (mut.) ELAC1 without (lanes 1-4) or with (lanes 5-8) 100 nM TRNT1 as indicated. Reactions were analyzed by TBE-urea-PAGE and SYBR Gold staining. Yellow arrowhead denotes altered migration of tRNAs after conversion of the 2',3'>p to 2'-OH and 3'-OH groups by T4 PNK. Red arrowheads denote complete re-addition of the 3'CCA nucleotides by TRNT1. Note that instead of only removing the 2',3'>p as T4 PNK does (lane 2), ELAC1 cleaves off the extra two nucleotides following the discriminator base to regenerate ΔCCA tRNA (lane 3). TRNT1 is able to fully add back the 3'CCA to both ELAC1-modified products (lane 7). However, after T4 PNK treatment, TRNT1 is only able to efficiently add back the terminal 3' adenine at position 76 to ΔCCA + CC and not ΔCCA + AA (lane 6). **(G)** Radiolabeled untreated ΔCCA-HDV (top panel) or ΔCCA-HDV treated with either CNP to generate a 2' phosphate (2'-p) or RtcB to generate a 3' phosphate (3'-p) (bottom panels) as in Fig. **1B** was incubated with 100 nM TRNT1 and the indicated enzymes. Reactions were analyzed by SDS-PAGE and autoradiography. Note that ELAC1 is able to convert all three ΔCCA tRNAs into substrates for CCA addition by TRNT1.

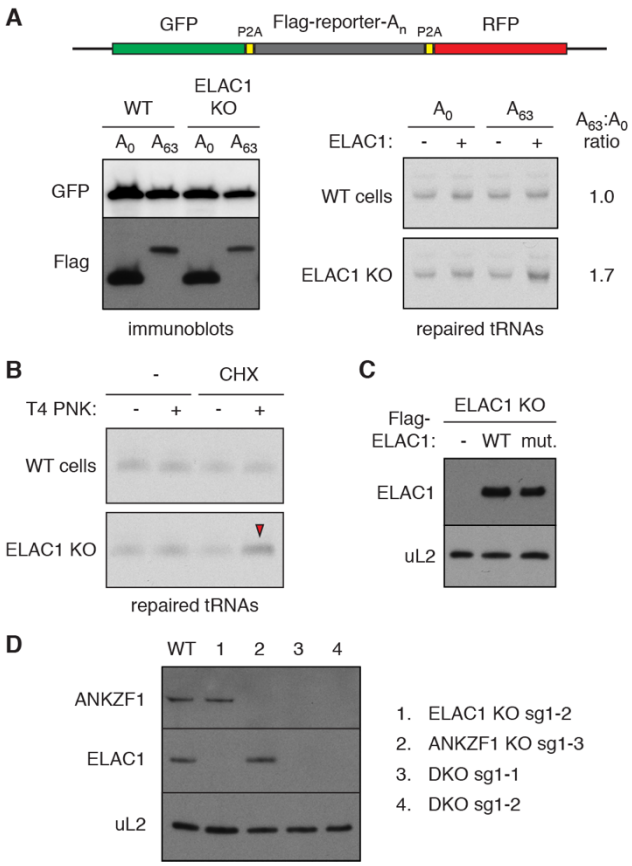

Figure S4. ELAC1 recycles tRNAs downstream of RQC in cells (related to Fig. 4). (A) WT or ELAC1 KO (sg1-2) cells were transfected with reporter constructs (top) encoding either no (A0) or a stall-inducing stretch of 63 (A63) adenine residues behind a Flag-tagged peptide. Expression of an N-terminal GFP released by a self-cleaving viral P2A peptide and the Flag-tagged reporter protein was assayed by SDS-PAGE and immunoblotting (bottom, left). RNAs harvested from lysates were then incubated with 0.2 mM [α-33P]-CTP and 100 nM TRNT1 without or with 20 nM ELAC1 to radiolabel repaired tRNAs as in Fig. **4B**. Intensity of labeled tRNAs was quantified, and the ratio of labeling with ELAC1 was normalized for poly(A)-expressing cells to control cells. Increased labeling is observed selectively in ELAC1 knockout cells overexpressing the poly(A63) reporter. **(B)** RNA isolated from wildtype (WT) or ELAC1 knockout (KO; sg1-2) HEK293T cells treated as in Fig. **4B** was incubated with 0.2 mM [α-33P]-CTP, 100 nM TRNT1 without or with 0.375 U/µL T4 PNK and analyzed by SDS-PAGE and autoradiography. This shows that labeling of tRNA intermediates specifically increases in ELAC1 KO cells treated with cycloheximide (CHX) in the presence of T4 PNK. **(C)** Lysates isolated from ELAC1 KO cells re-expressing nothing, wildtype, or H64A Flag-tagged ELAC1 were subject to immunoblotting. Quantified results from two biological replicates (one shown here) are in Fig. **4C**. **(D)** Immunoblotting for the indicated components in WT, ANKZF1 KO, ELAC1 KO, and ELAC1/ANKZF1 double knockout (DKO) cell lines.

Table S1. Mass spectrometry protein identification hits (related to Fig. 1)

Uniprot ID	Gene name	Unique peptides	Total peptides
G1T8R1	RAP1GAP2	11	14
G1U3R6	RAP1GAP2	7	15
G1SDU6	TARS	7	9
G1T2I4	EPRS	6	10
G1SVJ5	SARS	5	7
P11909	GPX1	5	6
P68105	EEF1A1	3	6
G1T7Z0	PGD	3	3
Q71V39	EEF1A2	3	3
G1SIV7	NARS	2	3
G1SK30	MTRR	2	3
G1T846	DARS	2	3
G1SQ02	PRDX1	2	2
G1T3Z5	CDV3	1	3
G1SF46	UBB	1	2
G1SSK8	CS	1	2
G1SEM5	ZFAND6	1	1
G1SNB9	ANGPTL1	1	1
G1SW46	RNASEH2B	1	1
G1SXC7	ELAC1	1	1
G1SZ91	FABP5	1	1
G1TM81	TPT1	1	1
P08628	TXN	1	1